STUDY ON THE IMPACT OF NEAR-WALL AIR SYSTEMS' WIND SPEED VARIATIONS ON THE COMBUSTION CHARACTERISTICS IN COAL-FIRED BOILERS

by

Lihua CAI[a,b*], Wangyongjia ZHONG[a], Dianxu RUAN[c], Xiangfei LIN[d], and Haifeng FANG[a,b]

[a]College of Mechanical Engineering, Jiangsu University of Science & Technology, Zhenjiang, Jiangsu, China
[b]Suzhou Institute of Technology, Jiangsu University of Science & Technology, Suzhou, Jiangsu, China
[c]Shazhou Professional Institute of Technology, Suzhou, Jiangsu, China
[d]Jiangsu Shengang Boiler Co., Ltd., Suzhou, Jiangsu, China

Original scientific paper
https://doi.org/10.2298/TSCI251113021C

With increasingly strict national energy policies mandating ultra-low emissions for coal-fired power plants, the issue of high temperature corrosion caused by reductive gases and elevated furnace temperatures has become critical. This study proposes the implementation of near-wall air systems on both sides of mid-furnace burners to mitigate water-cooled wall corrosion and enhance combustion efficiency. Using numerical simulation, the effects of a near-wall air system with a wind speed of 20 m/s were analyzed across the entire furnace. Results show that this approach reduces the average near-wall temperature by 4%, while increasing O_2 concentration in the combustion zone by approximately 6%, thus promoting more efficient combustion. Additionally, CO_2 and CO concentrations decrease by about 4.5% and 5.9%, respectively, effectively reducing reductive gases and alleviating high-temperature corrosion. The NO_x decreased significantly by 18.7%, indicating that air classification effectively suppressed NO_x, which is a sign of efficient and low-nitrogen combustion. These findings offer a practical solution for improving boiler operational safety and efficiency under ultra-low emission requirements.

Keywords: *pulverized-coal boiler, tangential firing, near-wall wind technology, CFD, NO_x emission*

Introduction

Currently, the low-NO_x combustion technologies adopted by pulverized coal boiler manufacturers face certain challenges. Specifically, during the application of these technologies [1], the water-cooled walls in the burner area of boilers may suffer from corrosion under high temperatures [2], leading to phenomena such as furnace slagging or the formation of corrosion pits on the water-cooled walls [3]. Water-cooled wall high temperature corrosion can result in decreased tube strength and thinning of the wall thickness [4], posing significant impacts on the

*Corresponding author, e-mail: justcailihua@163.com

safe and economical operation of boilers [5]. To further unveil the mechanisms of water-cooled wall high temperature corrosion, scholars both domestically and internationally have conducted a series of studies in this field [6]. Research by Shim *et al*. [7] indicates that vapor-phase sulfide attack, accumulation of unburned fuel and impurities, and chloride attack are the primary causes of water-cooled wall high temperature corrosion. Xiong *et al*. [8] investigated the causes of high temperature corrosion in the water-cooled walls of a typical 300 MW class boiler, discovering that excessive sulfur content in coal and an oversized virtual circle diameter of primary air are the fundamental reasons for water-cooled wall high temperature corrosion.

According to existing studies, the high temperature corrosion of boiler walls results from the interaction between corrosive gases and deposits in combustion products with the metal surface [9]. The core mechanisms include the formation of a corrosive atmosphere, catalytic effects of deposits, disruption of the oxide layer, and chemical corrosion of the metal substrate [10]. It is evident that high temperature corrosion of water-cooled walls in boilers is a complex phenomenon involving coal quality, equipment design, and operational aspects [11]. Understanding its causes and impacts, and implementing appropriate control measures are essential for ensuring the safe and stable operation of boilers [12].

To mitigate the phenomenon of high temperature corrosion in boilers, scholars both domestically and internationally have proposed solutions, primarily including optimizing water-cooled wall tube materials, applying anti-corrosion coatings to heated surfaces, and optimizing combustion adjustments [13]. However, the optimization of water-cooled wall tube materials cannot ensure the high temperature resistance and anti-corrosion performance at the welds of low-alloy and high-alloy steels [14], employing anti-corrosion coating technology results in relatively thin coatings that offer limited protection against high-temperature corrosion over shorter periods [15], and combustion adjustment methods for boilers can also lead to a reduction in the reducing atmosphere at the water-cooled walls to minimal values, with limited adjustment capabilities [16].

Therefore, considering the limitations and drawbacks of the aforementioned technologies, various scholars have found during research that the near-wall air system (NWAS) can effectively reduce the risk of high temperature corrosion on boiler heating surfaces through cooling, dilution, and scouring effects [17]. Moreover, compared to other retrofit technologies such as air staging and fuel reburning, NWAS involves relatively lower modification costs, shorter construction periods, and does not require extensive modifications to the burner structure, making it easier to implement. At the same time, due to the power consumption of its auxiliary equipment is much lower than the economic loss caused by unplanned furnace shutdowns due to corrosion. Therefore, installing a NWAS on the boiler is an effective solution to alleviate high temperature corrosion. However, the NWAS limited adoption is due to the lack of standardized design rules, conservative industry practices, and insufficient long-term validation. Continuous modeling improvement and on-site demonstrations are crucial for gaining the confidence of regulatory authorities and operators in extensive industrial deployment. The original intention of this study is precisely to systematically verify the feasibility of NWAS technology in pulverized coal boilers through high-precision numerical simulation. Therefore, in practical applications, combustion efficiency, wear, and other factors must be comprehensively considered to rationally design and adjust NWAS parameters to achieve optimal performance [18].

Certainly, with continuous improvements in computer performance and numerical simulation methods, researchers now rely on computational tools to explore the effectiveness of near-wall air technology [19], simulating the combustion process in furnaces equipped with

NWAS to obtain corresponding simulation results [20]. Zhao and Ming [21] conducted detailed studies on furnace combustion, investigating pulverized coal combustion and heat transfer models. Ettouati *et al*. [22] established a furnace model for a swirling pulverized coal burner boiler, performed combustion simulations, and validated the results experimentally. Li *et al*. [23] carried out a numerical study in a 600 MW wall-tangentially-fired boiler using a newly proposed combustion mechanism to evaluate the effects of oxy-fuel combustion conditions and biomass blending ratios on flow, temperature, O_2 distribution, and burnout behavior. Yao *et al*. [24] investigated the combustion characteristics of a 660 MW tangentially-fired pulverized coal boiler under different loads and burner arrangements. Ma *et al*. [25] further studied the impact of a newly designed separated over-fire air (SOFA) plenum on boiler performance for a 300 MW coal-fired power plant boiler burning low-volatile coal, and based on this, proposed an optimized SOFA plenum design. Additionally, Wen *et al*. [26] investigated the influence of different near-wall air ratios on furnace combustion characteristics for a 650 MW supercritical opposed-swirl combustion boiler suffering from water-wall high temperature corrosion. By comprehensively considering corrosion protection effectiveness, modification cost, and emission constraints, they determined 2.6% as the optimal near-wall air ratio. Yu *et al.* [27] conducted numerical simulations using CFD software to analyze the in-furnace velocity, temperature, and species distribution under near-wall air conditions for a 300 MW subcritical drum boiler.

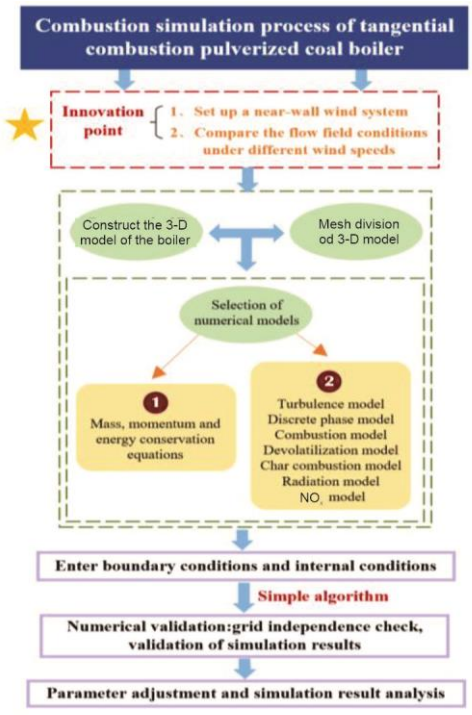

Figure 1. Overall research methodology

In summary of the aforementioned literature, it can be observed that the installation of NWAS is effective for preventing high temperature corrosion of water-cooled walls, and numerical simulation serves as a crucial method for studying this issue in utility boilers [28]. However, existing studies on near-wall air technology are not comprehensive. They merely discuss the differences in furnace flow fields before and after introducing near-wall air technology [29], without further investigating how various wind speeds within a reasonable range affect outcomes differently [30]. Additionally, their comparative analysis lacks detailed data. Therefore, the primary objective of this paper is to conduct a systematic and comprehensive study based on the introduction of near-wall air technology into boilers. Using CFD software, numerical simulations were performed for four different near-wall air velocities, analyzing in-furnace velocity, temperature, and species distributions [31]. Several representative sections from the main combustion zone and burnout zone of the furnace were selected to focus on the impact of near-wall air on the planar tangential circle, side wall area, and the reducing atmosphere throughout the entire furnace. By comparing various data points, the optimal injection wind speed for the NWAS in 300 MW pulverized coal boilers was determined, providing detailed references

for future boiler industries selecting parameters for NWAS. Figure 1 outlines the detailed research approach.

Computational details

Boiler specifications

This study investigates a 350 MW tangentially fired coal boiler at a Jiangsu power plant, measuring 66.6 m in height with a 20 m × 20 m cross-section. Through optimized air distribution and combustion organization, the boiler achieves low NO_x emissions compliant with strict environmental standards. Each corner includes five coal burners, six secondary air nozzles, and four overfire air nozzles. High and fluctuating temperatures in central burner zones promote alkali-induced high temperature corrosion. To mitigate this, NAWS was installed beside central C and E burners. A square nozzle design was adopted for meshing simplicity in numerical simulations. Figure 2 is a schematic diagram illustrating the specific structure of the boiler.

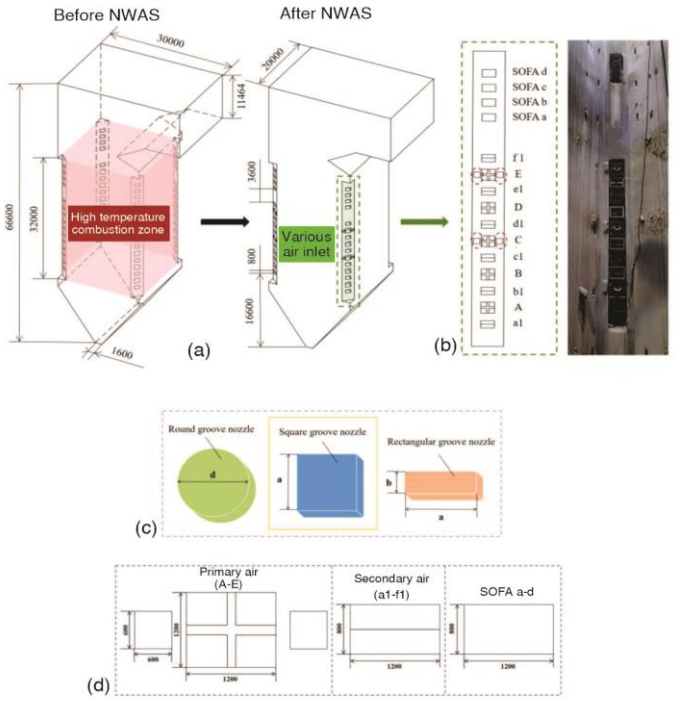

Figure 2. Boiler structure diagram; (a) boiler geometry, (b) burners and near-wall air nozzles layout diagram and site drawing, (c) wall air nozzle selection, and (d) schematic diagram of the specific dimensions of each air inlet

Operational details

The furnace employs tangential firing to implement air- and fuel-staging, thereby intensifying combustion efficiency. Figure 3(a) depicts the corner-wise injection trajectories of primary air, secondary air, SOFA and near-wall air. In the design of this boiler, the nozzles for

primary air, secondary air and burn-out air are all arranged at a certain angle towards the center of the furnace to enhance the disturbance of the air-flow and the mixing of combustion. The near-wall air nozzles are installed tangentially parallel to the water-cooled wall to form an adherent air-flow, which is used to prevent high temperature corrosion and cool the wall surface. Figure 3(b) contrasts the flow fields produced by two tangential-injection angles in a four-corner, pulverized-coal boiler.

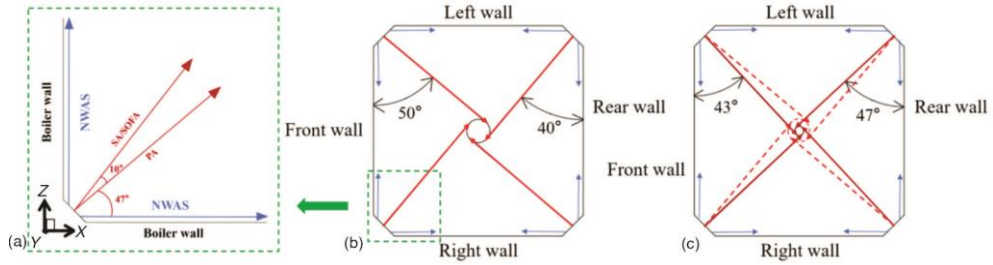

Figure 3. Diagram of incident wind angle; (a) schematic diagram of wall-mounted air supply and (b) schematic diagram of two jets with different tangential angles

By simulating a furnace deprived of near-wall air, we quantified the sensitivity of temperature and velocity fields to the wind-injection angle. At 40°, an excessive swirl develops, fig. 4: the flame tilts, corner uniformity deteriorates, and residual rotation persists. In contrast, the 47° tangent circle produces a markedly more centrosymmetric distribution of both temperature and velocity. This observation, corroborated by the reference plant data, rationalizes the adoption of the 47° configuration and underpins the fidelity of the simulation.

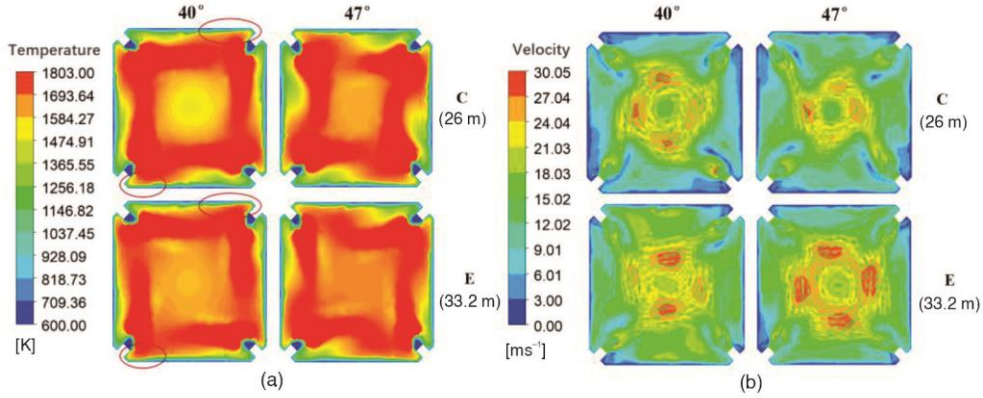

Figure 4. Comparison diagram of tangent circle simulation from different angles; (a) temperature simulation contour of the *zx*-plane cross-sections for burner C and E and (b) velocity-vector simulation of the *zx*-plane cross-section for burner C and E

Given that the primary objective of this study is to investigate the combustion process within the furnace, an appropriate simplification of the overall boiler model has been implemented. Additionally, the complex geometries of the burner nozzles have been simplified into rectangular shapes with similar dimensions for ease of modeling and analysis. The characteristics of the coal samples utilized in this study are summarized in tab. 1, while the performance parameters are detailed in tab. 2.

Table 1. Sample characteristics of the coal

Proximate analysis (wt.%, as-received basis)				Ultimate analysis (wt.%, as-received basis)					Net heating value (MJ/kg)
Volatile matter	Ash	Moisture	Fixed carbon	Carbon	Hydrogen	Nitrogen	Oxygen	Sulfur	
20.95	34.17	7.5	37.38	79.68	5.02	1.34	13.34	0.62	18.56

Table 2. Various performance parameters

Name	Boiler maximum continue rate
Superheater steam flow rate [th^{-1}]	999
Superheater steam outlet pressure [Mpa]	17.42
Superheater steam outlet temperature [K]	541
Reheater steam flow rate [th^{-1}]	955
Reheater steam inlet pressure [Mpa]	4.201
Reheater steam outlet pressure [Mpa]	4.011
Reheater steam inlet temperature [K]	341
Reheater steam outlet temperature [K]	541
Feed water temperature [K[	280
Actual fuel consumption [th^{-1}]	231.49
Boiler calculation of thermal efficiency [%]	93.41

Numerical simulation

Mathematical models and numerical algorithms

Boiler operation involves complex interactions of multiphase flow, combustion, and heat transfer. As analytical solutions are often unavailable for the governing equations, numerical simulations become essential [32]. The modeling framework typically includes turbulence, discrete phase, combustion, volatilization, char combustion, radiative heat transfer, and NO_x formation models.

Turbulence model

The boiler studied in this paper employs a swirl burner, which exhibits strong swirl characteristics. Therefore, the realizable k-ε model with swirl correction was selected [33]. The mathematical equations for the realizable k-ε model are as:

$$\frac{\partial}{\partial t}(\rho k)+\frac{\partial}{\partial X_i}(\rho k u_i)=\frac{\partial}{\partial X_j}\left[\left(u+\frac{u_t}{\sigma_k}\right)\frac{\partial k}{\partial X_j}\right]+G_{\mathrm{k}}+G_{\mathrm{b}}-\rho\varepsilon-Y_M+S_k \tag{1}$$

$$\frac{\partial}{\partial t}(\rho\varepsilon)+\frac{\partial}{\partial X_i}(\rho\varepsilon u_i)=-\frac{\partial}{\partial X_j}\left[\left(u+\frac{u_l}{\sigma_\varepsilon}\right)\frac{\partial k}{\partial X_j}\right]-\rho C_{2\varepsilon}\frac{\varepsilon^2}{k}+C_{1\varepsilon}\frac{\varepsilon}{k}(G_{\mathrm{k}}+C_{3\varepsilon}G_{\mathrm{b}})+S_\varepsilon \tag{2}$$

$$\sigma_k,\ \sigma_\varepsilon$$

where k is turbulent kinetic energy, ε – the dissipation rate of turbulent kinetic energy, G_{k} – the turbulent kinetic energy generated by mean velocity gradients, G_{b} – the turbulent kinetic energy due to buoyancy, Y_M – the effect of compressible turbulence pulsation expansion, $C_{1\varepsilon}$, $C_{2\varepsilon}$, $C_{3\varepsilon}$ – the empirical constants, S_k, S_ε – the source terms.

Discrete phase model

This study employs a discrete phase model based on the Euler-Lagrange approach. The particle trajectories are calculated using the stochastic orbit model [34]. By analyzing the force balance of coal particles in the flow field, the motion equation for coal particles can be expressed as:

$$\frac{\mathrm{d}u_\mathrm{p}}{\mathrm{d}t} = F_D(u - u_\mathrm{p}) + \frac{g_x(\rho_\mathrm{p} - \rho)}{\rho_\mathrm{p}} + F_x \tag{3}$$

$$F_D = -\frac{18\mu}{\rho_\mathrm{p} d_\mathrm{p}^{\,2}} \frac{C_D R_\mathrm{e}}{24} \tag{4}$$

where F_x is the additional term, $F_D(u - u_\mathrm{p})$ – the ratio of the particle mass to the drag coefficient, u – the fluid velocity, μ – the molecular viscosity of the fluid, ρ – the additional term, u_p – the particle velocity, ρ_p – the particle density, and d_p – the particle diameter.

Combustion model

Since the flame formed by coal particles after being ejected from the swirl burner and combusted in the furnace is a turbulent diffusion flame, this study selects the non-premixed combustion model to simulate the gas-phase combustion of coal particles. The influence of turbulence is considered using the probability density function method [35].

The mathematical expression for the mixture fraction is:

$$f = \frac{Z_i - Z_{i,\mathrm{ox}}}{Z_{i,\mathrm{fuel}} - Z_{i,\mathrm{ox}}} \tag{5}$$

where Z_i is the mass of element i.

Under identical diffusivity, the averaged mixture fraction equation can be expressed as:

$$\frac{\partial}{\partial t}\left(\rho\overline{f}\right) + \nabla\left(\rho\overline{v}\overline{f}\right) = \nabla\left(\frac{\mu_t}{\sigma_t}\overline{v}\overline{f}\right) + S_\mathrm{m} + S_\mathrm{user} \tag{6}$$

where S_user is the user-defined source term and S_m – the mass of coal particles transferred into the gas phase.

Devolatilization model

To ensure the accuracy of the computational results, this study employs a dual-competition reaction rate model, which can more accurately describe the reaction kinetics in systems involving two or more competing reactions. The specific model expression is as:

$$R_1 = A_1 \mathrm{e}^{-(E_1/\mathrm{R}T_P)} \tag{7}$$

$$R_2 = A_2 \mathrm{e}^{-(E_2/\mathrm{R}T_P)} \tag{8}$$

where R_1, R_2 are the reaction rate coefficients for volatile release at different temperatures, which are determined by the following formulas [36].

Under identical diffusivity, the averaged mixture fraction equation can be expressed as:

$$\frac{m_\mathrm{v}(t)}{(1 - f_{\mathrm{w},0})m_{\mathrm{p},0} - m_\mathrm{a}} = \int_0^t (\alpha_1 R_1 + \alpha_2 R_2) \exp\left\{-\int_0^t (R_1 + R_2)\mathrm{d}t\right\}\mathrm{d}t \tag{9}$$

where $m_v(t)$ is the mass of volatiles released at time t, m_a – the mass of ash in the coal particles, α_1, α_2 – the generation factors, and R_1 – the initial mass of the coal particles [37].

Char combustion model

In combustion science, the gas-solid surface reactions during char combustion are divided into different regimes depending on the temperature [38]. This study employs a kinetics/diffusion model to simulate char combustion.

The expression for the rate of oxygen diffusion to the char surface is:

$$D_0 = C_1 \frac{\left(\frac{T_p + T_\infty}{2}\right)^{0.75}}{d_p} \tag{10}$$

The expression for the chemical reaction rate at the char surface is:

$$R = C_2 e^{-(E/RT_p)} \tag{11}$$

where C_1 is the diffusion rate constant at the char surface, C_2 – the chemical reaction rate constant at the char surface, T_∞ – the ambient temperature, and E – the activation energy of the chemical reaction.

By combining the oxygen diffusion rate and the chemical reaction rate using a weighted average method [39], the expression for the overall char surface reaction combustion rate is:

$$\frac{dm_p}{d_t} = -Ap \frac{\rho R T_\infty Y_{ox}}{M_{w,ox}} \frac{D_0 R}{D_0 + R} \tag{12}$$

where $P_{ox} = (\rho R T_\infty Y_{ox})/M_{w,ox}$ is the partial pressure of the gaseous oxidant around the particle and R – the reaction constant obtained by combining the oxygen diffusion rate and the chemical reaction rate using a weighted average method. In this study, pulverized coal combustion is simulated using a species transport model coupled with global reaction mechanisms, without resolving the internal diffusion of moisture and volatiles within particles. This simplification may slightly affect the prediction of local ignition delay, but under the furnace's high temperature (>1300 °C) and well-mixed conditions, its impact on the overall temperature field and burnout efficiency is negligible.

Radiative heat transfer model

The majority of the heat absorbed by the water walls inside the boiler is obtained through flame radiation. This study employs the P-1 model to simulate radiative heat transfer within the furnace [40]. The specific equation for describing the radiative heat flux is as:

$$q_r = -\frac{1}{3(a + \sigma_s) - C\sigma_s} \nabla G \tag{13}$$

$$-\nabla q_r = aG - 4a\sigma T^4 \tag{14}$$

where a is the absorption coefficient, σ_s – the scattering coefficient, σ – the constant term, with a value of 5.67×10^{-8} W/m^{2}K^4, employed in calculating blackbody radiation, C – the coefficient of the linear anisotropic phase function, typically ranging from 0.1 to 0.2, and G – the incident radiative flux.

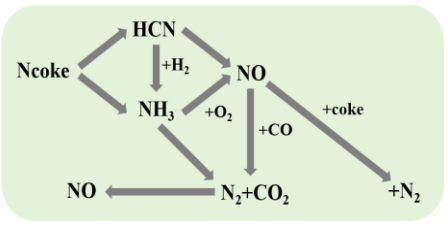

Figure 5. The nitrogen conversion pathways during combustion

The NO_x formation model

Due to the low NO_x content compared to total flue gases, post-processing is an effective method for simulating NO_x formation [41]. This study first simulates the full combustion process, then calculates NO_x based on the converged flow field. The NO_x is classified into prompt, thermal, and fuel types. As prompt NO_x is minimal, this work focuses on thermal and fuel NO_x. Figure 5 illustrates the nitrogen conversion pathways during combustion, including the formation and transformation processes of intermediate products such as HCN/NH_3, and highlights the influence of CO in these processes [42].

– Thermal NO_x

Thermal NO_x is predominantly formed through the oxidation of nitrogen in air under high-temperature conditions within the furnace [43]. The reaction mechanism is illustrated by:

$$O + N_2 \underset{K_{r1}}{\overset{K_{f1}}{\longleftrightarrow}} N + NO \tag{15}$$

$$N + O_2 \underset{K_{r2}}{\overset{K_{f2}}{\longleftrightarrow}} O + NO \tag{16}$$

$$N + OH \underset{K_{r3}}{\overset{K_{f3}}{\longleftrightarrow}} H + NO \tag{17}$$

where K_f, K_r are the forward and reverse reaction rates, respectively. The transport equation for thermal NO_x is:

$$\frac{\partial}{\partial t}\left(\rho Y_{NO}\right) + \nabla\left(\rho \bar{v} Y_{NO}\right) = \nabla\left(\rho D \nabla Y_{NO}\right) + S_{NO} \tag{18}$$

– Fuel NO_x

Fuel NO_x originates from the nitrogen content in coal powder during combustion, and its formation is primarily influenced by the proportion of nitrogen present in volatiles and char [44]. The nitrogen in volatiles undergoes decomposition into intermediates such as HCN and NH_3, which subsequently react with oxygen in the flue gas to form NO and N_2. Meanwhile, char not only directly oxidizes to produce NO but also reduces a portion of NO back to N_2 through heterogeneous reactions.

The reaction mechanism governing fuel NO_x formation can be expressed as:

$$HCN + O_2 \xrightarrow{K_4} NO + \cdots \tag{19}$$

$$HCN + NO_2 \xrightarrow{K_5} N_2 + \cdots \tag{20}$$

$$NH_3 + O_2 \xrightarrow{K_6} NO + \cdots \tag{21}$$

$$NH_3 + NO \xrightarrow{K_7} N_2 + \cdots \tag{22}$$

$$char + NO \xrightarrow{K_{char}} N_2 + \cdots \tag{23}$$

This model employs a post-processing method, and its accuracy satisfies the requirements of engineering practice. The calculated NO_x levels are also in good agreement with actual operating conditions.

Boundary condition

According to the actual specifications and operating conditions of the boiler, tab. 3 summarizes the wind temperatures, turbulence intensities, and hydraulic diameters set for each nozzle. The introduced NWAS is injected directly adjacent to the walls into the furnace interior. The optimal NWAS velocity will be determined through comparison with subsequent simulation results. Figure 6 illustrates the schematic diagram of the wind speed settings for each nozzle before and after introducing the NWAS. The inlet types for primary air, secondary air, SOFA, and NWAS are all defined as mass inlets, while the furnace outlet is set as a pressure outlet with a value of –20 Pa. All other walls of the boiler are defined as no-slip fixed walls, with a wall temperature set at 600 K.

Table 3. Specific parameters set for the nozzle

Inlet	Temperature [K]	Flow rate [kgs^{-1}]	Turbulence intensity [%]	Hydraulic diameter [mm]
Primary air	370	80	15	300
Secondary air	600	120	20	550
SOFA air	600	40	15	600
Near-wall air	473	30	20	450

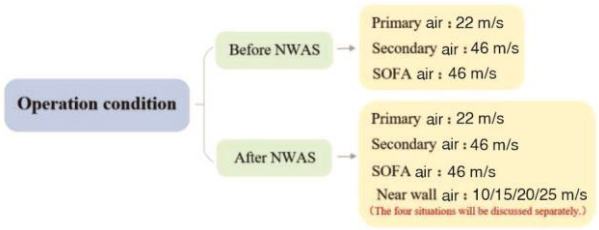

Figure 6. Operating condition diagram

During operation, the coal powder particles are modeled with a Rosin-Rammler (R-R) distribution, characterized by an average diameter of 75 μm and a distribution index of 1.5. The coal particle size distribution (PSD) in this study is fitted from plant-measured data using the R-R model. Although PSD can influence combustion characteristics, the present work focuses on evaluating the performance of the NWAS under practical operating conditions. Sensitivity analysis of PSD will be included in future studies on multi-coal adaptability. The pressure interpolation scheme employs the standard format, while all other governing equations are solved using a second-order upwind differencing scheme. The convergence criteria for the continuity and energy equations are set to less than 10^{-6}, whereas for the remaining equations, the residuals are required to be less than 10^{-3}.

Grid independence verification

To reduce computational costs, the simulation domain is limited to the horizontal duct and hopper. An unstructured tetrahedral mesh was employed for its advantages in handling complex geometries, local refinement, and multi-physics coupling. Surface size refinement was applied near nozzles to enhance mesh quality. The boiler mesh configuration is shown in fig. 7(a). While finer meshes generally improve accuracy, excessive element counts increase computational cost without yielding significant gains beyond a certain threshold [45].

To ensure mesh independence and minimize discretization errors, this study evaluated mesh counts of 1231457, 1586709, and 1961130. Results from different mesh resolutions

are shown in fig. 7(b), with fig. 7(c) displaying the highest and lowest quality fractions and their associated errors. At 1586709 elements, the average furnace temperature remained nearly constant vertically, showing the highest quality fraction and smallest error. Further refinement to 1961130 elements yielded no significant improvement. Therefore, a mesh count of 1586709 was selected as the optimal solution considering accuracy and computational cost.

After setting up all models and parameter conditions, numerical simulation techniques were employed to simulate the flow field within the entire boiler. The term *before NWAS* is used to denote the system configuration without NWAS injection. Subsequent comparison and analysis of the simulation results led to the following conclusions.

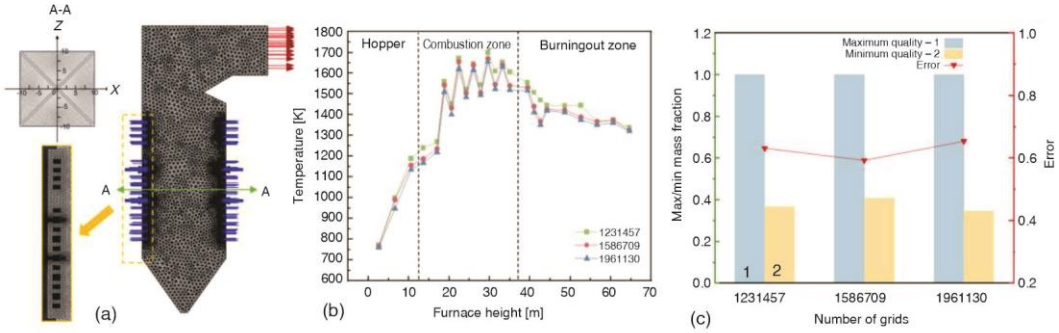

Figure 7. Mesh independence verification

Simulation result analysis

Model verification

In this study, an operational boiler from a power plant in Jiangsu was selected as the subject. Before introducing the NWAS, the measured values from the furnace were compared with the simulation results. Table 4 shows that the deviations are small, validating the accuracy of the simulation method. The differences mainly stem from the idealized assumptions made in the simulations versus the complexities of real-world operating conditions, as well as potential factors such as air leakage and uneven fuel distribution at the site. However, these deviations fall within an acceptable engineering range and do not affect the qualitative analysis and optimization studies of combustion characteristics and pollutant formation trends.

Table 4. Model validation values

Parameter	Actual furnace	Simulated furnace
Temperature [K]	1918	1871
O_2 [%]	14.91	15.23
CO_2 [%]	15.89	16.14
CO [%]	7.54	7.61

The entire furnace flow field was numerically simulated under design conditions, providing detailed temperature, velocity, and component distribution data. Mid-section burners were selected for analysis due to their ability to represent various operating conditions and yield comprehensive results. Burners C and E were chosen as reference cross-sections, as their simulation outcomes were comparable. A SOFA nozzle cross-section was also analyzed to enhance data reliability and support the simulation's validity. Contour plots of the furnace cross-section before and after NWAS implementation were used to assess its effectiveness in

mitigating high-temperature wall corrosion. This process also helped determine the optimal near-wall air injection velocity.

Temperature distribution

The temperature field distribution affects boiler combustion efficiency and wall slagging. As shown in fig. 8, coal powder and overfire air introduced from the four corners generate a ring-shaped high-temperature zone through volatile release and combustion.

As depicted in fig. 8, the introduction of the NWAS alters the airflow distribution in the vicinity of the burners. The near-wall air creates a cooling airflow layer adjacent to the walls, while the high-temperature flame region contracts toward the center, resulting in an increase in the average temperature across the burner cross-section.

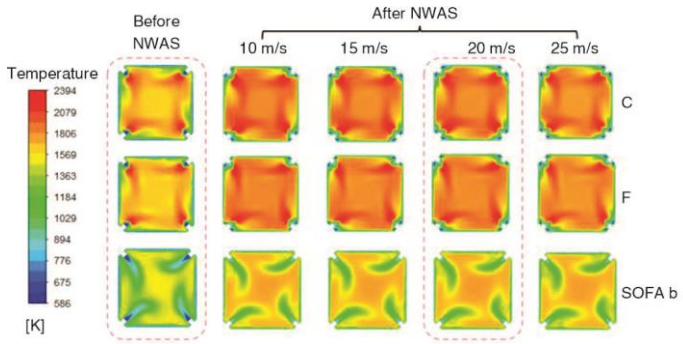

Figure 8. Temperature distribution

Velocity distribution

The velocity field governs the residence time of coal powder within the furnace, thereby influencing the completeness of combustion. A well-designed velocity field can enhance combustion efficiency, optimize temperature distribution, and assist in reducing NO_x emissions. Figure 9 illustrates the velocity distribution across various cross-sections of the furnace.

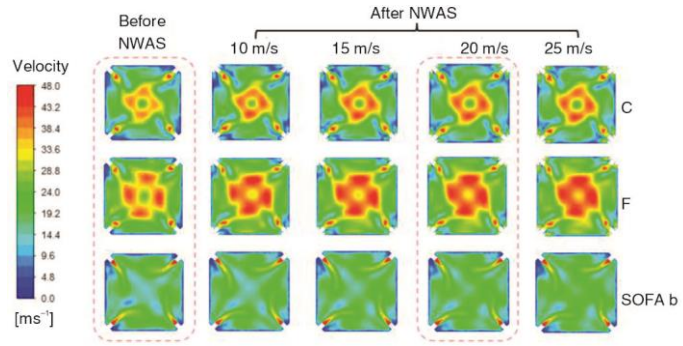

Figure 9. Velocity distribution

In the burner region, corner inlets generate a stable swirling flow with a centrally located vortex. The NWAS enhances central airflow concentration and intensity. Increased velocity improves flame stability, especially under low-load conditions, reducing the risk of flame detachment or extinction.

Species concentration distribution

Variations in composition field affect fuel–air mixing efficiency, influencing combustion performance. Proper mixing enhances combustion efficiency, reduces incomplete combustion losses, and minimizes slagging and fouling, thereby improving boiler operation. Composition analysis is therefore essential in boiler simulation studies.

The O_2 concentration

Proper coordination of air and coal powder is essential for enhancing the economical operation of boilers. Within a certain range, increasing the operating oxygen level can improve the contact and mixing between fuel and air, promoting complete combustion and reducing heat losses from incomplete combustion of both gaseous and solid fuels. As shown in fig. 10, the introduction of near-wall air reduces the oxygen concentration near the walls, thereby forcing combustion reactions to concentrate more in the central region of the burners. This concentrated combustion effect enhances overall combustion efficiency.

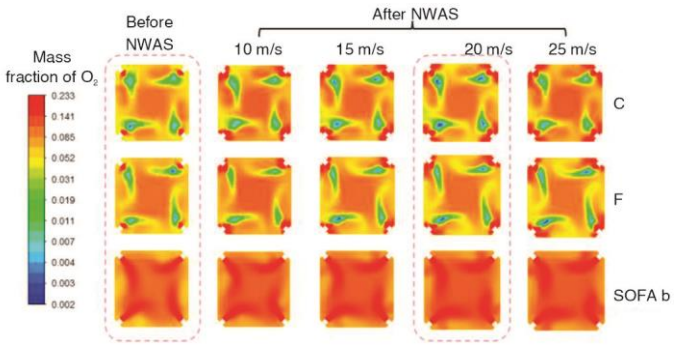

Figure 10. The O_2 distribution

The CO_2 concentration

High concentrations of CO_2 may indicate low oxygen levels during combustion, which can reduce combustion efficiency and lead to incomplete fuel combustion. Additionally, high concentrations of CO_2 dissolved in water produce carbonic acid, increasing the acidity of the water system and thereby accelerating equipment corrosion. This can result in scaling issues, negatively impacting heat transfer efficiency. As shown in fig. 11, after introducing the

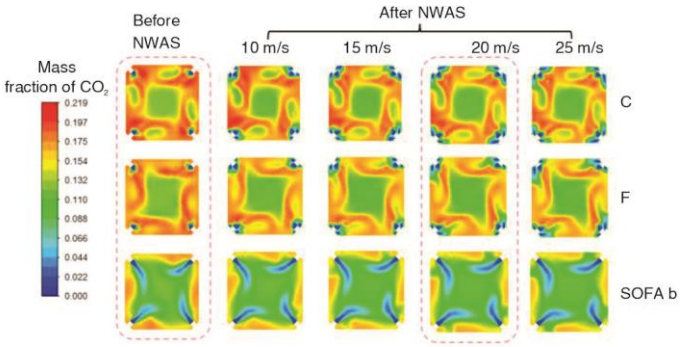

Figure 11. The CO_2 distribution

NWAS, the CO_2 concentration at the walls significantly decreases. The reduction in the volume fraction of CO_2 mainly results from the increase in flue gas volume and the rearward shift of the combustion zone, rather than a decrease in carbon conversion rate. This reduction is beneficial for preventing high-temperature corrosion and improving overall system longevity.

The CO concentration

The impact of CO concentration on boiler combustion is multifaceted, affecting combustion efficiency, energy utilization, environmental protection, and personal safety. Therefore, it is imperative to implement effective measures during the design and operation phases of boilers to control the formation and emission of carbon monoxide. As illustrated in fig. 12, the introduction of the NWAS leads to a significant reduction in CO content within the furnace. This improvement not only enhances combustion performance but also contributes to safer and more environmentally friendly operations.

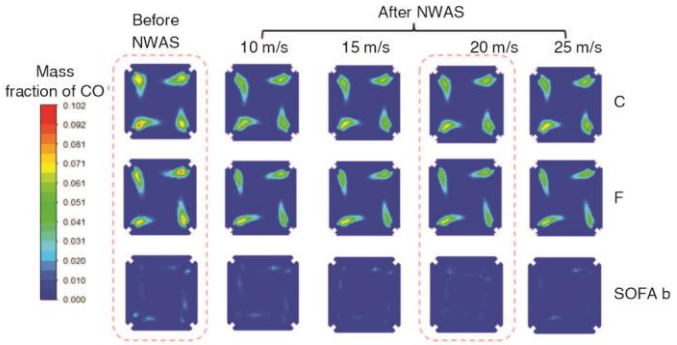

Figure 12. The CO distribution

The aforementioned findings indicate that the introduction of the NWAS effectively regulates the internal composition of the boiler, playing a crucial role in mitigating high temperature corrosion.

Overall contrastive analysis

Figures 8-12 show that the NWAS effectively mitigates high temperature corrosion by improving the temperature, velocity, and composition fields. The system achieves an optimal flow field state. As can be seen from fig. 13(a), the aggregated data is collected from the bottom of the boiler, with 24 monitoring sections selected from the bottom up. The heights of the sections selected for the ash hopper area, combustion area, and burnout area all maintain a certain regularity to ensure the reliability of the monitoring surface. Figures 13(b)-13(f) further explains the different conditions of the flow field in the furnace under different near-wall air velocities. This study systematically simulated four near-wall wind speeds (10-25 m/s), evaluating performance in terms of near-wall conditions, burnout, and flow stability. At 20 m/s, fly ash carbon content was minimized (2.0%), with uniform temperature and O_2 distribution, no CO accumulation, and a stable flame. In contrast, 25 m/s increased carbon content to 3.3%. Thus, 20 m/s achieves optimal combustion efficiency while effectively suppressing corrosion, representing the best overall performance.

Figure 14 compares furnace cross-section simulation results before and after implementing the NWAS. The results show more complete combustion, lower wall temperatures,

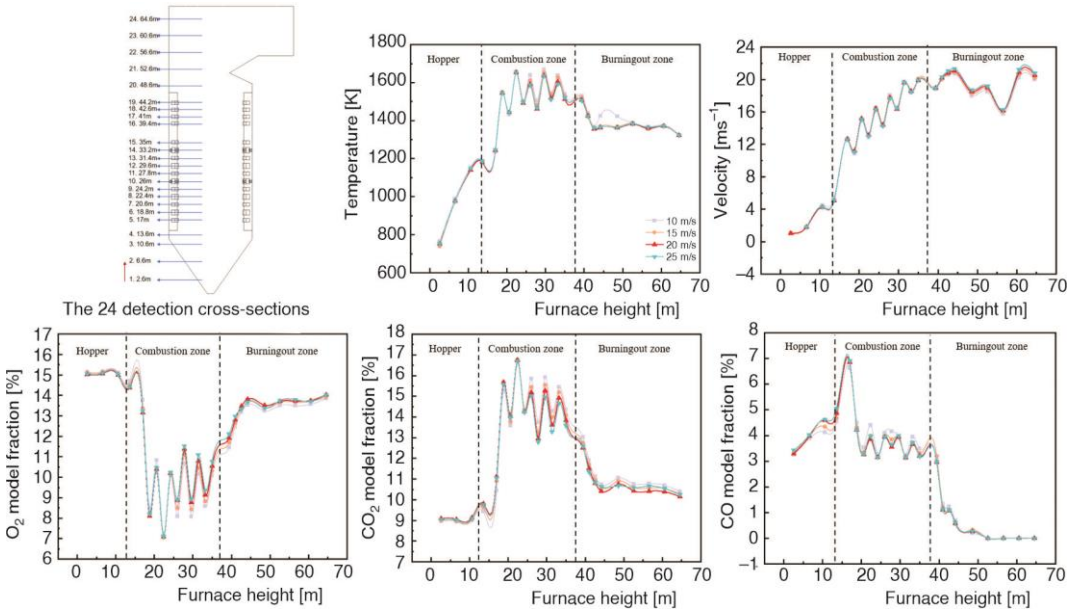

Figure 13. Plot of the influence of different near-wall wind speed on each factor

more concentrated central airflow, and a more uniform oxygen distribution without excessive peaks. CO_2 concentration is notably reduced both in the furnace and near the walls.

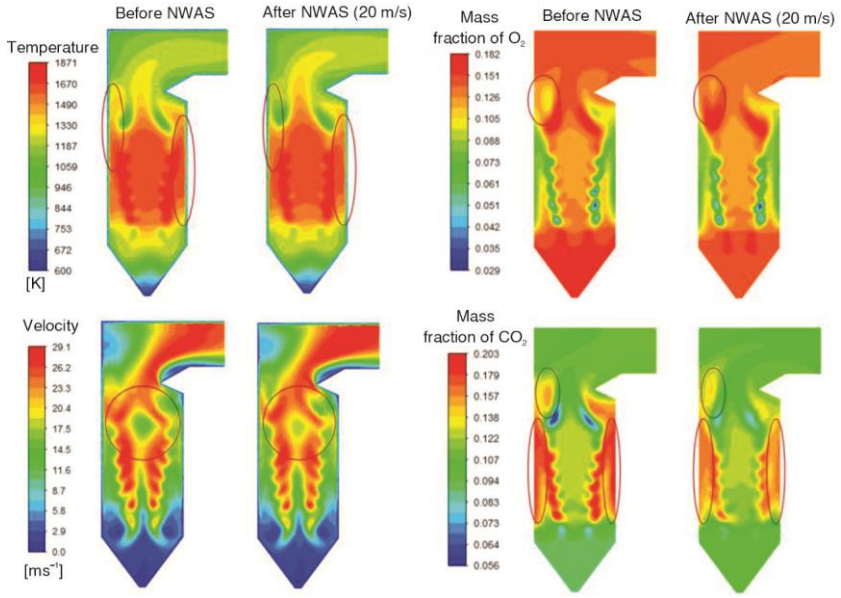

Figure 14. Simulation comparison of furnace cross sections before and after the introduction of near-wall wind system

Variations in NO_x emissions reflect changes in combustion conditions that can influence high temperature corrosion. Therefore, monitoring NO_x levels after implementing the NWAS is critical. As shown in fig. 15, simulation results indicate a significant decrease in NO_x

concentration between the main combustion zone and the water-cooled walls. This reduction improves the near-wall gas environment by lowering corrosive gas levels, thereby effectively mitigating high temperature corrosion of the boiler walls.

Figure 16 presents a numerical comparison demonstrating that the NWAS significantly enhances thermal uniformity in the furnace. The average furnace temperature decreases by nearly 4%, with the peak temperature dropping by approximately 100 K, effectively mitigating high temperature corrosion. Optimizing the air supply velocity to 20 m/s results in a more uniform distribution of both velocity and concentration

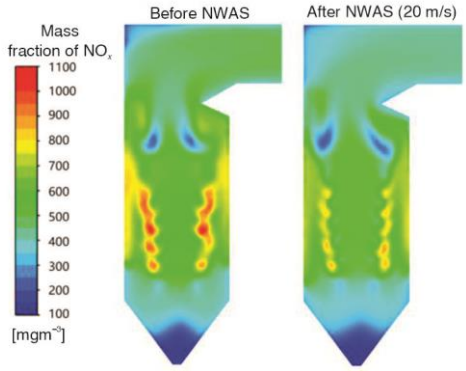

Figure 15. Simulation contour map of NO_x concentration distribution in the entire furnace

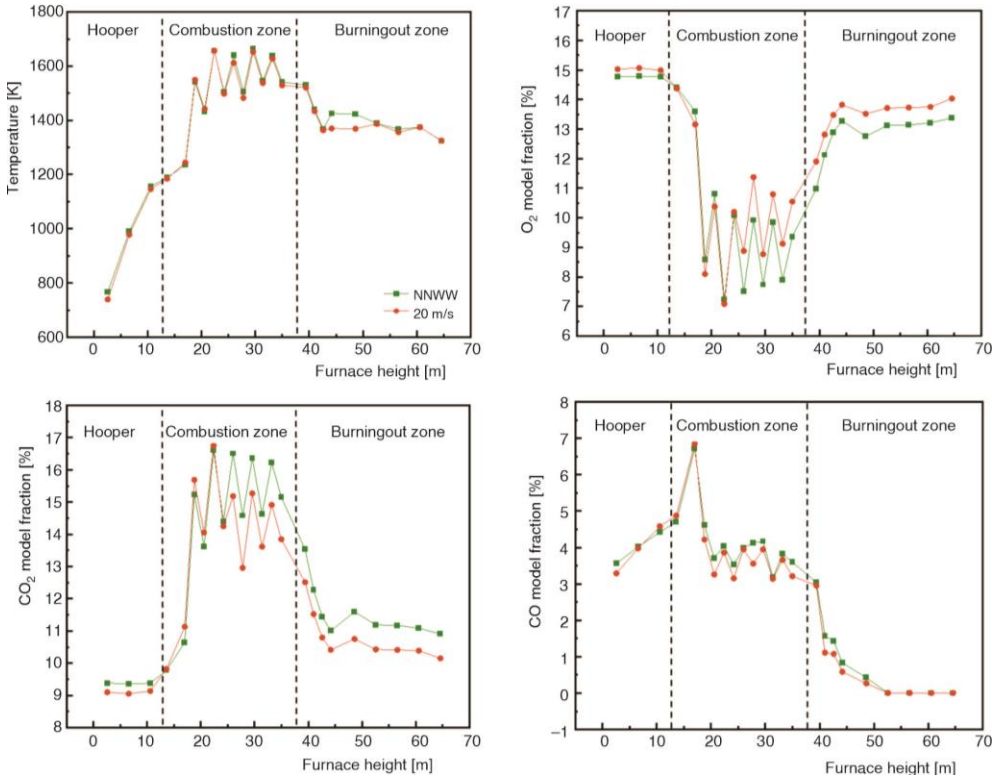

Figure 16. Simulation numerical comparison line chart

fields. Oxygen levels decrease in the hopper and burnout zones but increase by nearly 6% in the combustion zone, promoting more complete fuel oxidation. Additionally, the average CO_2 and CO concentrations throughout the furnace are reduced by 4.5% and 5.9%, respectively, indicating improved combustion efficiency and lower pollutant emissions. Table 5 is a comparison error table of the average gas concentrations in the central *xy* cross-section of the furnace. It vis-

Table 5. Comparison of combustion and emission characteristics before and after NWAS optimization

Detection position		Before NWAS	After NWAS (20m/s)	Change
Flue Gas Composition (dry basis, at furnace exit)	O_2 [%]	15.23	16.14	+6%
	CO_2 [%]	14.57	13.91	–4.5%
	NO_x [mgm^{-3}]	594.6	482.9	–18.7%
	SO_2 [mgm^{-3}]	46.82	35.96	–23.19%
Peak Near-wall (vol%, wet)	CO [%]	4.27	4.02	–5.9%

Note: O_2, CO_2, NO_x, and SO_2 are volume-weighted average values at the furnace exit. CO represents the maximum local concentration in the near-wall region, indicating the intensity of reducing conditions

ually presents the changes in various components after the introduction of the NWAS, particularly highlighting the reduction in reducing atmosphere components (such as CO) and corrosion-related components (such as SO_2). Therefore, it is evident that introducing a NWAS with an air velocity of 20 m/s on the boiler sidewalls can enhance the overall performance of the boiler.

Conclusions

This study numerically simulates the flow field of a 350 MW tangentially fired pulverized coal boiler using ANSYS Fluent, with a focus on the effects of introducing the NWAS at varying wind speeds. By comparing the temperature, velocity, and species concentration fields before and after system implementation, key findings were obtained.

- Distribution trends of O_2, CO_2, and CO vary under different conditions. In the combustion zone, O_2 concentration inversely correlates with that of CO_2 and CO. O_2 levels are higher in the horizontal flue, while CO is nearly zero. CO_2 peaks in the main combustion zone.
- The NWAS significantly increases O_2 concentration near the furnace walls while reducing CO_2 and CO levels, thereby mitigating high temperature corrosion risks.
- The addition of this system reduces extreme high temperature zones. Overall, boiler NO_x concentration drops by 18.7%, with outlet NO_x also noticeably reduced.
- Analysis of four different injection speeds for the NWAS shows 20 m/s as optimal across all sections.

Future research could explore additional factors such as different injection angles or temperatures of the near-wall air, aiming to further refine and optimize the parameters of the NWAS. Additionally, investigations could focus on the shape of the near-wall air nozzles, comparing simulation results at the nozzle injection points.

Nomenclature

A_1,A_2 – reaction rate constant [s^{-1}]
a – absorption coefficient [m^{-1}]
C – coefficient of the linear anisotropic phase function
C_1,C_2 – rate constant [ms^{-1}]
$C_{1\varepsilon}$,$C_{2\varepsilon}$,$C_{3\varepsilon}$ – empirical constants
d_p – particle diameter [m]
E_1,E_2 – activation energy [Jmol^{-1}]
F – additional term [kgm^{-3}]
f – mixed fraction
G – incident radiative flux [Wm^{-2}]
G_b – turbulent kinetic energy due to buoyancy [m^{2}s^{-3}]
G_k – turbulent kinetic energy generated by mean velocity gradients [m^{2}s^{-3}]
K_f,K_r – forward and reverse reaction rates [s^{-1}]
k – turbulent kinetic energy [m^{2}s^{-2}]
$m_v(t)$ – mass of the volatile substance released at time t [kg]
q_r – radiant heat flux [Wm^{-2}]
R_1,R_2 – reaction rate coefficients for volatile release at different temperatures [s^{-1}]
R_o – initial coal particle mass [kg]
S_k,S_ε – defined source terms [m^{2}s^{-3}]

s – scattering coefficient [m^{-1}]
T – temperature [K]
T_∞ – ambient temperature [K]
u – fluid velocity [ms^{-1}]
Y_M – effect of compressible turbulence pulsation expansion
Z_i – mass of element i

Greek symbols

α_1,α_2 – generation factors
ε – dissipation rate of turbulent kinetic energy [m^2s^{-3}]
μ – molecular viscosity of the fluid [Pa·s]
ρ – additional term
σ_k,σ_ε – diffusion coefficient in the turbulence model

Acronyms

NWAS – near-wall air system
PSD – particle size distribution
R-R – Rosin-Rammler
SOFA – separated over-fire air
WTFB – wall-tangentially-fired boiler

Data availability statement

All data, models, and code generated or used during the study appear in the submitted article.

Disclosure of potential conflicts of interest

The authors report no conflict of interest.

Funding

This work has been funded by [1] Qing Lan Project of the Higher Education Institutions of Jiangsu Province and [2] Postgraduate Research & Practice Innovation Program of Jiangsu Province (SJCX25_2535).

Notes on contributors

– Lihua Cai, female, doctor, associate professor, master's supervisor, the main contributions is: Writing – review & editing.
– Wangyongjia Zhong, female, graduate student, the main contributions is: Writing – original draft.
– Dianxu Ruan, male, senior engineer, the main contributions is: Conceptualization.
– Xiangfei lin, male, engineer, senior engineer, the main contributions is: Methodology.
– Haifeng Fang, male, doctor, professor, master's supervisor, the main contributions is: Supervision.

References

[1] Wang, J., Research Status and Progress of Natural Gas Low-Nitrogen Combustion Technology, *Modern Chemical Industry*, *42* (2022), S2, pp. 47-50
[2] Ke, H., *et al*., Cause Analysis and Preventive Measures for Boiler Water Wall Leakage in 350 MW Unit of a Thermal Power Plant, *Die & Mould Manufacture, 25* (2025), 07, pp. 247-249
[3] Juncheng, X., *et al*., Simulation Research on Thermal Management System of Battery Module with Fin Heat Dissipation Structure, *Applied Thermal Engineering, 239* (2024), 122177
[4] Ke, C., Analysis of the Principle of High-Temperature Corrosion of Water-Cooled Walls in Supercritical Boilers and the Problem of Wall-Adhering Air Modification, *Science and Technology & Innovation*, *12* (2025), 9, pp. 229-232
[5] Tao, Q., Wang, Y., Analysis of Causes and Prevention of High-Temperature Corrosion in the Water-Cooled Walls of a 1000 MW Corner-Tangential Coal-Fired Boiler, *Mechanical and Electrical Information, 18* (2023), pp. 62-66
[6] Liu, T., *et al*., Numerical Investigation of Stable Combustion at Ultra-Low Load for a 350 MW Wall Tangentially Fired Pulverized-Coal Boiler: Effect of Burner Adjustments and Methane Co-Firing, *Applied Thermal Engineering, 246* (2024), 122980

[7] Shim, H.-S., *et al*., Development of Fireside Waterwall Corrosion Correlations Using Pilot-Scale Test Furnace, *Fuel, 87* (2008), 15/16, pp. 3353-3361
[8] Xiaohe, X., *et al*., Water Wall Tubes' High Temperature Corrosion Root Cause Investigation: A 300 MW Level Boiler Case, *Energies, 16* (2023), 4, pp. 1767-1767
[9] Bai, F., High Temperature Corrosion Analysis and Treatment Measures of Water Wall of 600 MW Subcritical Pulverized Coal Boiler, *Power System Engineering, 40* (2024), 03, pp. 52-54+57
[10] Zhenhua, Y., *et al*., An Innovative Low-NO_x Combustion Technology for Industrial Pulverized Coal Boiler: Gas-Particle Flow Characteristics with Different Radial-Air-Staged Levels, *Energy, 260* (2022), 125142
[11] Wei, J., *et al*., Numerical Study on the Effects of Primary Air Ratio on Ultra-Low-Load Combustion Characteristics of a 1050 MW Coal-Fired Boiler Considering High-Temperature Corrosion, *Applied Thermal Engineering, 221* (2023), 119811
[12] Xu, S., *et al*., Study on High Temperature Corrosion Mechanism of Water Wall Tubes of 350 MW Supercritical Unit, *Engineering Failure Analysis, 121* (2021), 105131
[13] Yunfei, S., *et al*., Cause Analysis of Corrosion and Burst of Water Wall of Utility Boiler, *Journal of Physics: Conference Series, 2399* (2022), 1, 012031
[14] Zixiang, L., *et al*., A Novel Burner Arrangement Scheme with Annularly Combined Multiple Airflows for Wall-Tangentially Fired Pulverized Coal Boiler, *Energy, 222* (2021), 119912
[15] Qiu, Z., Jianxin, Q., Mechanism Analysis for High-Temperature Corrosion Behaviors of Boiler Water-Wall Tube and Its Arc Spraying NiCr Coating in a Power Plant, *Thermal Power Generation, 53* (2024.), 07, pp. 143-148
[16] Xie, P., Xu, L., The Analysis on the Causes of the Water Wall Pipe Burst in Industrial Boilers, *Journal of Engineering Mechanics and Machinery, 8* (2023), 1, 080102.
[17] Yue, J., Huang, J., Analysis and Prevention of High-Temperature Corrosion in the Water-Cooled Walls of a 1000 MW Ultra-Supercritical Double-Opposed-Firing π-Shaped Pulverized Coal Boiler, *Energy Research and Utilization*, 36 (2024), 03, pp. 35-39
[18] Xue, W., *et al*., Influences of Operation Parameters on Blended Combustion Zhundong Coal in 330 MW Coal-Fired Boilers, *Journal of University of Jinan (Science and Technology), 37* (2023), 03, pp. 380-388
[19] Xiaohe, X., *et al*., Water Wall Tubes' High Temperature Corrosion Root Cause Investigation: A 300 MW Level Boiler Case, *Energies, 16* (2023), 4, pp. 1767-1767
[20] Ma, H., *et al*., Design of Porous Wall Air Coupling with Air Staged Furnace for Preventing High Temperature Corrosion and Reducing NO_x Emissions, *Applied Thermal Engineering, 124* (2017), Sept., pp. 865-870
[21] Zhao, L. Z., Ming, F. Y., Numerical Simulation of the Effects of Charge Stratification on Combustion and Emissions, *Energy & Fuels, 21* (2007), 4, pp. 2018-2026
[22] Ettouati, H., *et al*., Numerical Modelling and Simulation of Pulverized Solid-Fuel Combustion in Swirl Burners, *The Canadian Journal of Chemical Engineering, 87* (2009), 3, pp. 350-358
[23] Li, D., *et al*., Numerical Study of Co-Firing Biomass with Lean Coal Under Air-Fuel and Oxy-Fuel Conditions in a Wall-Fired Utility Boiler, *Energy & Fuels, 31* (2017), 5, pp. 5344-5354
[24] Yao, L., *et al*., Influence of Closing-to-Wall Air on Combustion Process in 660 MW Opposed Firing Boiler, *Journal of Southeast University(Natural Science Edition), 45* (2015), 01, pp. 85-90
[25] Ma, L., *et al*., More Efficient and Environmentally Friendly Combustion of Low-Rank Coal in a Down-Fired Boiler by a Simple but Effective Optimization of Staged-Air Windbox, *Fuel Processing Technology, 194* (2019), 106118
[26] Wen, H., *et al*., Numerical Simulation and Practical Verification of Near-Wall Air System for an Ultra-Supercritical Boiler, *Electric Power Technology and Env. Protection, 41* (2025), 03, pp. 488-496
[27] Yu, Y., *et al*.,. Influence of Closing-to-Wall Air on Combustion in 300 MW Firing Boiler, *Boiler Manufacturing, 30* (2024), 02, pp. 16-18+21
[28] Chen, Q., *et al*., Numerical Simulation and Practical Verification of Near-Wall Air System for an Ultra-Supercritical Boiler, *Journal of Engineering for Thermal Energy and Power, 37* (2022.), 10, pp. 112-121
[29] Habib, M. A., *et al*., Computational Fluid Dynamic Simulation of Oxyfuel Combustion in Gas-Fired Water Tube Boilers, *Computers and Fluids, 56* (2012), pp. 152-165
[30] Mohamadreza, E., *et al*., CFD Simulation and Optimization of an Industrial Cement Gas-Solid Air Classifier, *Particuology, 89* (2024), June, pp. 172-184
[31] Zixiang, L., *et al*., Low Load Performance of Tangentially-Fired Boiler with Annularly Combined Multiple Airflows, *Energy, 224* (2021), 120131

[32] Weijuan, Y., *et al*., Effects of Near-Wall Air Application in a Pulverized-Coal 300 MWe Utility Boiler on Combustion and Corrosive Gases, *Energy & Fuels, 31* (2017), 9, pp. 10075-10081
[33] Lu, K., *et al*., Numerical Study on Combustion Characteristics of Wall-Type Tangential Boiler, *IOP Conference Series: Earth and Environmental Science, 237* (2019), 2, pp. 022043-022049
[34] Hyunbin, J., *et al*., Influence of Uneven Secondary Air Supply and Burner Tilt on Flow Pattern, Heat Transfer, and NO_x Emissions in a 500 MWe Tangential-Firing Coal Boiler, *Energies, 14* (2021), 24, pp. 8352-8352
[35] Hao, L., *et al*., Numerical Simulation of Combustion Characteristics in a 660 MW Tangentially Fired Pulverized Coal Boiler Subjected to Peak-Load Regulation, *Case Studies in Thermal Engineering, 49* (2023), 103168
[36] Yanyu, Q., *et al*., Combustion and NO_x Formation Characteristics from a 330 MWe Retrofitted Anthracite-Fired Utility Boiler with Swirl Burner Under Deeply-Staged-Combustion, *Energy, 258* (2022), 124832
[37] Bo, Z., *et al*., Study on Combustion Characteristics and NOx Formation in 600 MW Coal-Fired Boiler Based on Numerical Simulation, *Energies, 16* (2022), 1, pp. 262-262
[38] Dafu, M., *et al*.,. Combustion Stability and NO_x Emission Characteristics of Three Combustion Modes of Pulverized Coal Boilers Under Low or Ultra-Low Loads, *Applied Energy, 353* (2024), Part A, 121998
[39] Wang, J., *et al*., Numerical Simulation of a Decoupling and Reburning Combinative Low-NO_x Coal Grate Boiler, *Journal of Cleaner Production, 188* (2018), July, pp. 977-988
[40] Xu, S., *et al*., Simulation Study on Effect of New Combined Closing-to-Wall Air on High Temperature Corrosion Atmosphere of Boiler Water Wall, *Thermal Power Generation, 51* (2022), 04, pp. 79-87
[41] Huang, L., *et al*., Numerical Study on the Effect of the Over-Fire-Air to the Air Flow and Coal Combustion in a 670 t/h Wall-Fired Boiler, *Fuel Processing Technology, 87* (2005), 4, pp. 363-371
[42] Zeng, J., High Temperature Corrosion Analysis and Treatment of Water Wall of 350 MW Opposed Firing Boiler, *Industrial Boilers, 42* (2022), 01, pp. 51-53+62
[43] Pei, J., *et al*., Optimizing the Combustion of Low-Quality Coal by the Wall Wind Auxiliary Combustion Method in a Tangentially Fired Utility Boiler, *Combustion Science and Technology, 191* (2019), 3, pp. 570-589
[44] Si, W., *et al*., Combustion Performance and NO_x Emissions in a 330 MW Tangentially Fired Boiler Retrofitted with Preheating Combustion Devices, *Energy, 318* (2025), 134803
[45] Ling, S., *et al*., Optimization Study of Low-NO_x Combustion in Boiler Based on Pulverized Coal Preheating Solution, *Case Studies in Thermal Engineering, 65* (2025), 105647

Paper submitted: November 13, 2025
Paper revised: January 5, 2026
Paper accepted: January 29, 2026
2026 Published by the Vinča Institute of Nuclear Sciences, Belgrade, Serbia.
This is an open access article distributed under the CC BY 4.0 terms and conditions.